Catal Lett (2008) 123:65–71
DOI 10.1007/s10562-008-9394-8

Porogen Template Assisted TiO_2 Rutile Coupled Nanomaterials for Improved Visible and Solar Light Photocatalytic Applications

Mathieu Grandcolas · Maithaa Karkmaz-Le Du · Florence Bosc · Alain Louvet · Nicolas Keller · Valérie Keller

Received: 30 June 2007 / Accepted: 4 January 2008 / Published online: 23 January 2008
© Springer Science+Business Media, LLC 2008

Abstract The controlled synthesis, using Brij56, PEG, PVA and CTAB organic porogens, of TiO_2 rutile-coupled nanomaterials leads to efficient visible and solar light photocatalytic materials at room temperature. Examples are provided for the total oxidation of CO, the production of hydrogen from water splitting and the gas phase diethylsulfide degradation.

Keywords Photocatalysis · TiO_2 · Rutile · Anatase · WO_3 · Visible and solar light activation · Binary and ternary coupling

1 Introduction

During the last decades, research involving photocatalysis has gained considerable attention as a clean and environmentally friendly technology for water and air depollution, decontamination and desinfection, for fine chemical synthesis or in the field of alternative energy through hydrogen production. This led photocatalysis to recently move from basic to applied research. Unfortunately, the low solar light absorption of the most used and efficient photocatalyst, anatase TiO_2, is a serious drawback for many applications, only the near-UV part of the spectra being used, corresponding to about 4% of the solar spectrum. The development of photocatalysts with high efficiency under visible light ($\lambda > 380$ nm) should allow a larger part of the solar spectrum, and even the poor illumination of indoor lighting, to be used and thus transferring the activation mode from UV to visible light has become a hot-topic in photocatalysis. Different approaches for achieving this goal have been studied, such as the use of smaller band gap materials, the doping of TiO_2 crystals [1, 2], the generation of oxygen vacancies by forming reduced TiO_x [3], and the coupling of two semiconductors, usually TiO_2 and a visible-light activated one.

Beside the extensively studied anatase [4], its polymorphic rutile phase was generally limited to the cosmetic field, in plastics and white pigments, due to a good light-scattering and light-reflecting effect that protect material from UV light. In photocatalysis, much less attention has been paid to rutile than to anatase. However, rutile is a smaller band gap energy phase (3.0 eV) than the anatase (3.2 eV), and thus has been reported to exhibit interesting photocatalytic activity under visible or solar light [5], due to better photo-absorption properties and to a higher quantum yield in the beginning of the visible light range, as measured by Anpo for the hydrogenation of CH_3CCH with H_2O [6]. However, obtaining nanostructured rutile with good cristallinity and high surface area is more difficult than for anatase, due to the particle size-dependence thermodynamic stability of titania, anatase being more stable than rutile for particle diameters below 14 nm [7]. Usual syntheses by high temperature calcination of amorphous TiO_2 or anatase nanoparticles at temperatures greater than 500 °C, result in large sintered rutile crystallites with low surface area. Many

M. Grandcolas · M. Karkmaz-Le Du · F. Bosc · N. Keller · V. Keller (✉)
Laboratoire des Matériaux, Surfaces et Procédés pour la Catalyse (LMSPC), European Laboratory for Catalysis and Surface Sciences (ELCASS), CNRS, Louis Pasteur University, 25 rue Becquerel, Strasbourg 67087, France
e-mail: vkeller@chimie.u-strasbg.fr

N. Keller
e-mail: nkeller@chimie.u-strasbg.fr

A. Louvet
Délégation Générale à l'Armement (DGA), Centre d'Etude du Bouchet (CEB), BP 3, Vert-le-Petit 91710, France

studies have been devoted to the development of low temperature methods for preparing rutile nanoparticles, including e.g. hydrothermal [8] or supercritical drying methods [9]. Usually, there are few reports reporting the synthesis of stable rutile at low temperatures [10–12].

Preparing TiO_2 through template-assisted sol–gel methods allowed the obtention of large surface areas and of a structural control through uniform and tunable pore or channel creation. These structures result from specific organic–inorganic interactions between titanium species and the porogen template, usually organic polymers [13], ionic or nonionic surfactants [14], block polymers [15], or nonsurfactant templates [16]. Interesting nanostructural properties generally result from the template removal during a thermal post-synthesis treatment.

Amongst the different methods reported in literature to extend the light-absorbing property of anatase to the visible or solar light region of the spectra and to enhance its photocatalytic, one of the most promising way is to couple anatase with narrow band gap semi-conductors [17]. Tungsten-doped TiO_2 or WO_3-containing photocatalytic composites are of interest [18]. In this case, the coupling of two semi-conductors with different and suitable redox energy levels for both conduction and valence bands is an attractive approach to obtain visible and/or solar-light efficient photocatalysts.

Here, we report the porogen template-assisted sol–gel synthesis of high surface area coupled rutile-anatase materials, supporting WO_3 or metal particles, for visible/solar light activation, with tunable porosity network/surface area generated by the templating porogen. This synthesis is supported by the concept of the binary/ternary coupling of anatase with narrow band gap semiconductors such as rutile and WO_3 for extending the absorption to the visible spectra and improving the photocatalytic performances. Applications include the visible light CO oxidation, the visible and solar light gas phase diethylsulfide (DES) degradation and the hydrogen production by solar light photocatalytic water splitting.

2 Experimental

The visible-light active nanosized rutile-anatase photocatalysts were synthesized following a liquid phase low temperature dissolution-repricipitation process using a sol gel procedure in which titanium isopropoxide was first hydrolyzed by the addition of a 2 M HCl aqueous solution, followed by a 48 h aging of the obtained hydrosol [10]. The thermodynamically stable rutile phase with fine particle size can also be obtained after aging even at room temperature. Polyoxyethylene(10)cetyl ether (Brij 56), polyethylene glycol (PEG), cetyltrimethyl ammonium bromide (CTAB) or polyvinylalcohol (PVA) porogen templates were added after the aging step and the reactant mixture was dried at room temperature and further at 110 °C before the final treatment in air at 400 °C for 2 h. The rutile and anatase content was derived from the intensity of the most intense diffraction peaks, the (110) and (101) peaks at 27.6° and 25.4° respectively, according to the JCPDS files 21-1276 and 21-1275. Comparison was made with the commercial P25 TiO_2 reference (Degussa) with an anatase:rutile ratio of about 80:20 and a specific surface area of about 50 m^2/g.

For the CO oxidation and the hydrogen production, the platinum deposition was performed using an aqueous solution of H_2PtCl_6. After drying at 110 °C for 1 h in air, and oxidation at 350 °C for 1 h, the material was finally reduced in flowing hydrogen at 400 °C for 1 h. Palladium was co-impregnated using palladium nitrate, before drying and final temperature treatments. For the DES degradation, TiO_2 was impregnated with an aqueous solution of ammonium paratungstate pentahydrate. After drying at room temperature and further at 110 °C for 2 h, a final calcination was performed in air at 400 °C for 1 h in order to obtain the WO_3/TiO_2 coupled photocatalytic systems.

Gas phase photocatalysis was carried out in a tubular concentric Pyrex/quartz reactor made of two coaxial tubes between which the reactants were flowing. The catalyst was coated on the internal surface of the external tube. Details on the photoreactor can be found in previous works [19]. The catalyst was exposed to the reactant-containing air stream until dark-adsorption equilibrium was reached. The illumination, provided by commercial 8 W daylight (400–800 nm) lamps or solar simulating lamps, located inside the inner tube, was further switched on.

The liquid phase hydrogen production was carried out under a 110 mL/min nitrogen flow in a 1 L Pyrex reactor equipped with a plunging tube in which a 150 W metal halide lamp was located vertically. This tube was surrounded by a water circulation cylindrical Quartz jacket, in order to avoid the heating of the aqueous reactional media, and the reaction was performed under mechanical stirring.

For the DES degradation, the photocatalytic performances were derived from GC/MS analyses, whereas those observed in CO oxidation and hydrogen production were obtained by microGC.

3 Results and Discussion

It could be noted that the anatase-rutile ratio could be easily tuned from 100–0 (pure anatase) to 0–100 (pure rutile) depending on the aging duration, since the appearance of the rutile phase from pure anatase occurred only after 5 h of aging, with a constant hydrodynamic ratio

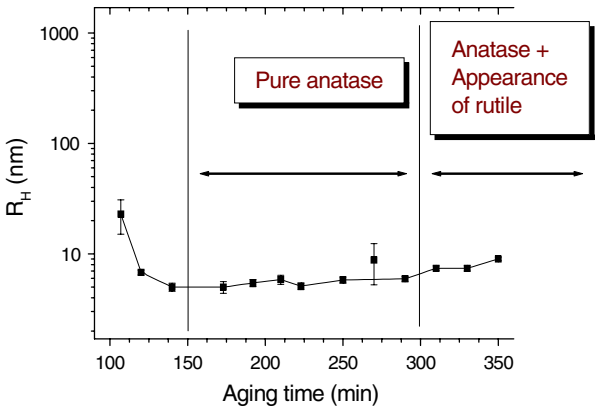

Fig. 1 Evolution of the hydrodynamic ratio and appearance of the rutile phase from pure anatase with the aging time

(Fig. 1). A previous work reported the interest of using a porogen agent for synthesizing rutile photocatalysts with suitable surface area, and pure rutile could be obtained after 48 h of aging using the PEG porogen [10]. However, for a same aging duration, the anatase-rutile ratio could be modified by acting on the nature of the porogen template: Figure 2 shows the XRD pattern of TiO_2 obtained using PEG, PVA, CTAB and Brij56 as porogens, compared to that of the 80/20 anatase/rutile TiO_2 P25 from Degussa. Table 1 reports the anatase-rutile ratio together with the specific surface area and the mean crystallite size as a function of the starting porogen template after 48 h aging. The nature of the porogen did not significantly influence the mean crystallite size, while its removal by decomposition during the final post-synthesis thermal treatment

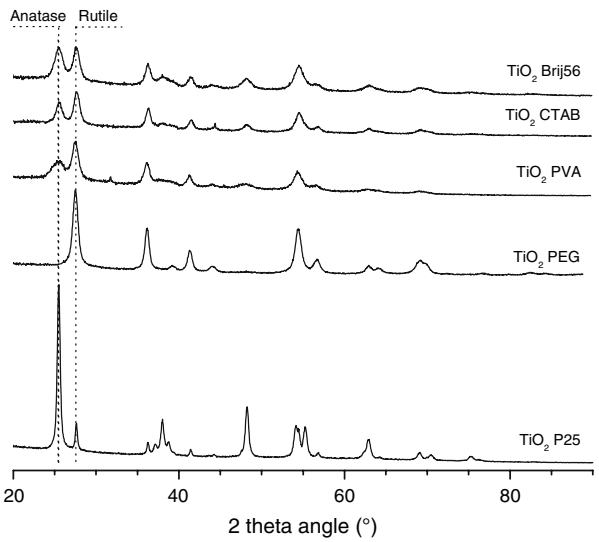

Fig. 2 X-ray diffraction diagrams of TiO_2 P25 and rutile-anatase nanosized TiO_2 materials obtained by different porogen-assisted sol–gel synthesis (PEG, PVA, CTAB and Brij 56). The most intense diffraction peaks of rutile and anatase phases, at 27.6° and 25.4° respectively, are marked in the diagrams

Table 1 Specific surface area, mean crystallite size diameter and anatase/rutile ratio, depending on the starting template after 48 h aging

Template	Specific surface area (m^2/g)	Crystallite size (nm)		Anatase: rutile ratio
		Anatase	Rutile	
PEG	120	–	11	0:100
PVA	150	9	10	30:70
Brij56	100	7	10	50:50
CTAB	70	11	10	40:60
Without template	30	/	10	0:100

acted on the specific surface area by creating porosity (Fig. 3). By comparison, a similar low temperature dissolution–reprecipitation process without template addition resulted in a lower specific surface area pure rutile material, with a flat pore size distribution profile, evidencing that the template played a role of porosity promoter. By contrast, the rutile content of the material could be tuned from pure rutile to 50/50 anatase-rutile, depending on the nature of the porogen. This was attributed to the specific interaction between the porogen template and the surface groups exposed by the nanocrystallites during the final thermal treatment.

Abe et al. have shown the interest of using a mixture of anatase and rutile photocatalysts for the hydrogen production by water splitting under UV-A illumination [20]. It could be noted here that by playing on the nature of the porogen template, anatase-rutile photocatalytic systems with intragranular instead of intergranular coupling could be obtained. A wide range of porogen templates could thus allow the crystallographic composition of the coupled TiO_2 photocatalytic material to be tuned. This intragranular location of both TiO_2 phases should provide an intimate contact between both oxide phases and improve the efficiency of the semiconductor coupling effect, according to

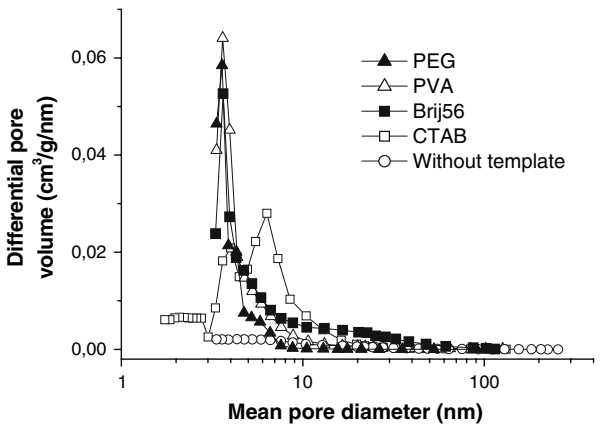

Fig. 3 Pore size distribution of rutile-anatase nanosized TiO_2 materials obtained by PEG, PVA, CTAB and Brij 56 porogen-assisted sol–gel synthesis

Wu et al. who found that the closer the contact between two titania phases the higher the photocatalytic activity of the catalyst for mechanically mixed biphase titania catalysts [21]. Indeed, it was also reported by Di Paola et al. that the coexistence of two semiconductors in the same particle (intra-grain coupling) led to the improvement of the photoactivity for the liquid phase photodegradation of phenol when compared to a simple mixture of the corresponding semiconductors (inter-grain coupling) [22]. They showed for WO_3–WS_2 systems that a composite consisting of WO_3 or WS_2 islands surrounded respectively by a WS_2 or WO_3 sea respectively, was more active than the corresponding mechanical mixture. The enhanced efficiency observed was attributed to more intimate contacts between WO_3 and WS_2, necessary to achieve an efficient charge separation, and thus high photocatalytic performances.

The resulting TiO_2 anatase/rutile coupled photocatalytic materials showed interesting shifts in visible-light absorption properties relatively to the TiO_2 P25 reference (Fig. 4).

3.1 *On-stream* CO oxidation

High performances for the visible-light CO oxidation have been obtained on template assisted TiO_2 rutile-coupled materials. Examples are given in Table 2 for concentrated (2000 and 4000 ppm) flowing CO oxidation on TiO_2 rutile (PEG) photocatalysts decorated with Pt(0.3 wt.%) or both Pt(0.3 wt%) and Pd(0.3 wt%) particles, and compared to the Pt/P25 analogue. Whatever the photocatalyst, total selectivity into CO_2 was obtained, and no significant CO oxidation was observed in the dark. For 2000 ppm of CO, the Pt(0.3%)/rutile photocatalyst displayed a total and stable CO conversion (over 3 days) with no CO release, while the Pt/P25 analogue reached 75% of conversion before rapidly deactivating on stream. A stable 96% oxidation efficiency was obtained on the Pt(0.3%)/rutile with 4000 ppm of CO, while rapid deactivation was observed on the Pt(0.3%)/P25 with a maximum conversion at 30%. Since the platinized catalyst based on pure sol-gel anatase displayed no activity under visible light illumination (not reported), the slight activity of the P25 TiO_2 resulted from its 20% rutile content, whereas the whole semi-conductor was activated in the rutile-PEG material.

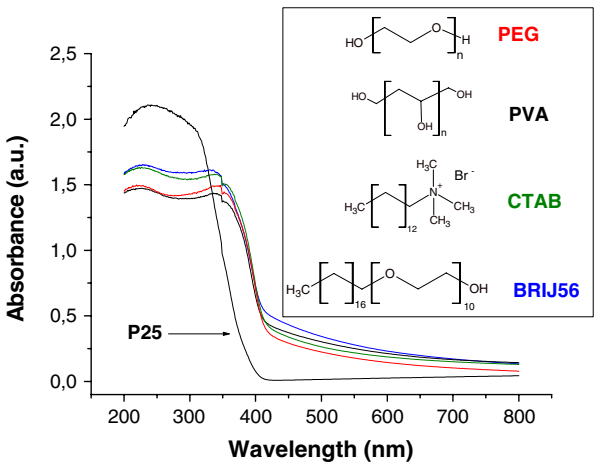

Fig. 4 Light absorption properties of TiO_2 anatase/rutile-based materials. Insert: the different porogen templates used

The deactivation shown by the commercial P25 could be explained as follows, without exclusive. On rutile-containing catalysts (P25 and synthesized rutile-based materials), the possible surface re-oxidation of metallic platinum nanoparticles ($Pt \rightarrow PtO_x$) resulting from the chemisorption of oxygen is overcome by the photogenerated electron transfer from the rutile conduction band to platinum under illumination. This would allow the platinum to be maintained in the metallic state at the rutile surface. By contrast, on the P25 photocatalyst, the fraction of the platinum particles located on the anatase could not maintain a metallic surface, because anatase could not be activated by visible-light wavelenghts, resulting in the on-stream gradual formation of surface PtO_x species with lower CO uptake. Thus only the adsorption of CO onto platinum located on the rutile could remain optimized. This was in agreement with the time on stream stability shown under UV-A illumination by the Pt/P25 photocatalyst (not shown).

The main role of platinum nanoparticles consists (i) in improving the photogenerated charge separation, electrons being transferred to the platinum whereas holes simultaneously accumulated at the metal–oxide interface [23], and (ii) in adsorbing CO, the very low CO adsorption on pure TiO_2 being a limiting factor to the CO photooxidation efficiency [24]. The CO uptake on Pt/TiO_2 has been optimized at 0.3 wt.% of platinum by CO adsorption measurements.

Decorating the Pt/rutile photocatalyst with 0.3 wt.% palladium allowed total and stable CO removal to be obtained for a 4000 ppm inlet concentration. Since palladium showed poor CO adsorption properties compared to platinum, decoration of platinum by palladium could further limit the charge recombinations by involving the palladium mainly in the photogenerated charge transfer process and not in the CO adsorption.

This showed that total CO oxidation can be achieved at room temperature under visible-light illumination, even for 4000 ppm of CO, without any particular restrictive limitations in the size of platinum or palladium particles as it is the case for gold-based thermal catalysts.

3.2 Diethylsulfide Degradation

Visible-light on-stream degradation of diethylsulfide (DES), which is commonly used as a model molecule for

Table 2 Performances for the on-stream room temperature CO oxidation with visible-light activation obtained on the high surface area rutile-PEG supported 0.3 wt.% platinum photocatalyst versus its Pt/P25 analogue. Influence of the palladium decoration

Catalyst nature	Inlet CO content, ppm	Maximum of CO conversion, %	Stability on stream
Pt/Rutile-PEG	2000	100	Over 3 days
Pt/Rutile-PEG	4000	96	Over 3 days
Pt/Rutile-PEG decorated with 0.3% Pd	4000	100	Over 3 days
Pt/P25	2000	74	Deactivation after 50 min on stream
Pt/P25	4000	30	Deactivation after 20 min on stream

Reaction conditions: 2000 or 4000 ppm CO, 50% relative humidity in balance air at a 200 mL/min total flow. 400 mg of photocatalyst corresponding to a 1 mg/cm^2 surface weight density coating

the Yperite chemical warfare agent (Mustard gas or 2,2′-dichloroethylsulfide) could be efficiently performed on different template-assisted WO_3 (4 wt.%) coupled TiO_2 anatase-rutile materials (Fig. 5a). The most efficient one, prepared using Brij56 as template porogen, showed both a high initial abatement (96%) and a steady state level (after more than 6 h on stream) around 47%, while the WO_3/P25 with coupled 80/20 anatase-rutile TiO_2 achieved only an initial abatement of 65% before deactivating to a steady state level of 40%. The positive effect of the coupling with WO_3 was observed by comparing the WO_3-based ternary system with the WO_3-free anatase-rutile TiO_2 obtained from Brij56, which displayed a strongly lower steady state DES abatement of 27%.

Since the anatase phase was not activated by the visible light in the anatase-rutile mixed system, one should expect that the increase of the visible light-active rutile content would result in the increase in the DES abatement efficiency. This was not observed on these systems, the PVA- and PEG-based photocatalysts only achieving a steady state DES abatement of 27% and 25% respectively, despite a rutile content of 70% and 100% respectively. The WO_3/TiO_2 anatase-rutile with 100% of rutile even displayed a totally different behavior on stream. Further analyses are required, but this evidences the interest of preparing mixed anatase-rutile materials with a suitable anatase-to-rutile ratio.

The deactivation of the photocatalysts with time on stream was attributed to the deposition of sulfate species resulting from the total oxidation of diethylsulfide. The presence of sulfur as sulfate at the catalyst surface was observed by X-ray photoelectron spectroscopy. This will be detailed in a forthcoming article devoted to the surface nature of used coupled photocatalysts.

Figure 5b shows the DES abatement obtained as a function of time under solar illumination over the different rutile-based coupled photocatalysts. It evidenced that high performances in solar light degradation was obtained, even higher than under visible light illumination. Indeed, the rutile-based coupled photocatalysts exhibited 100% DES removal during more than 2 h, before deactivating down to a steady state level of 53% after more than 6 h on stream.

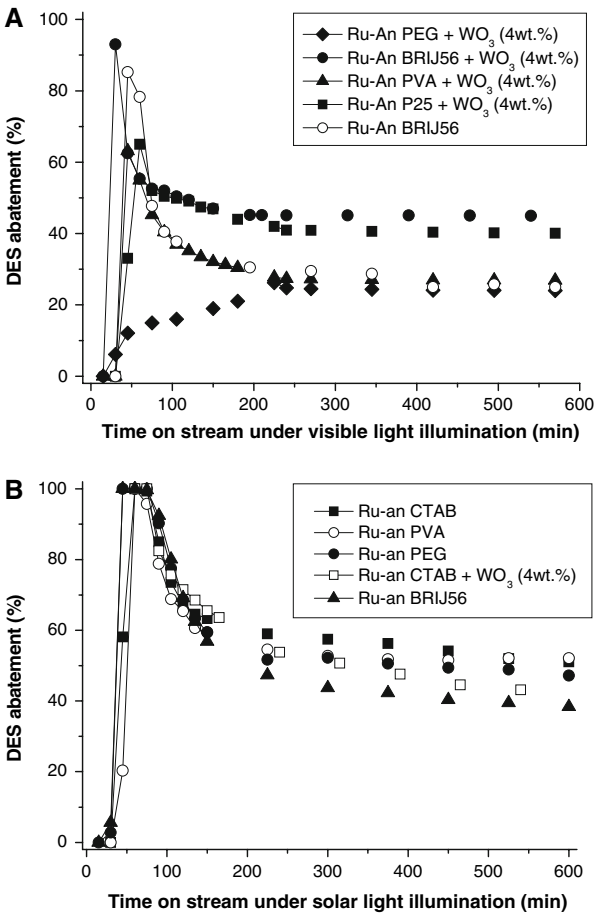

Fig. 5 8 W-visible light (**a**) and solar light (**b**) flowing (50 cc/min) diethylsulfide degradation on porogen template assisted coupled TiO_2 anatase/rutile photocatalysts. Reaction conditions: 370 ppm DES, 50% relative humidity in balance air at a 50 mL/min total flow. 400 mg of photocatalyst corresponding to a 1 mg/cm^2 surface weight density coating

3.3 Hydrogen Production

The photocatalytic production of hydrogen from solar light and water, as a source of clean energy targeting the aim of a sustainable development, has received much attention. These template assisted TiO_2 anatase/rutile-based photocatalysts not only find interesting applications in gas phase degradation of chemical pollutants but also in liquid phase hydrogen production. The solar-light driven water splitting for producing hydrogen can be put forwards as a high interest potential application of these nanomaterials (Fig. 6). In this case, different Pt-supported anatase-rutile template assisted materials have been tested, and the most efficient Pt(0.3 wt%)/anatase-rutile Brij56 catalyst led to significative and stable H_2 production with no deactivation over more than 3 days. Similarly to the behavior observed for the diethylsulfide degradation, the efficiency of the materials could not be directly correlated to the rutile or to the anatase content: the 100% and 70% rutile-based materials led to an hydrogen production of 18 µmol/min and 13 µmol/min respectively, whereas, by contrast, 26 µmol/min of hydrogen was produced over the 50/50 anatase-rutile based photocatalyst. Again, this example pointed out that a suitable and optimal anatase-rutile ratio should be obtained for optimizing the photocatalytic efficiency. Methanol (1:15 volume ratio to water) was used as sacrificial reactant for evidencing this phenomena.

Further works are ongoing to reduce the amount of methanol sacrificial reactant, to fully distinguish between hydrogen issued from methanol and that formed by water splitting, and to use hydrogen-free sacrificial agents.

Coupled TiO_2 rutile nanomaterials obtained by porogen template-assisted synthesis have been pointed out as promising photocatalysts for visible and solar light applications in the depollution field and for energetic purposes. Nanostructured mesoporous rutile TiO_2 with high specific surface area can be obtained using a template assisted low temperature dissolution–reprecipitation process, the nature of the template mainly allowing the rutile/anatase ratio to be tuned. The photocatalytic efficiency of the rutile materials could be improved by a binary or ternary coupling with other oxide semi-conductors like UV-A activated anatase TiO_2 and UV-A/visible light activated WO_3. Under solar illumination, all the studied oxides were activated whatever their natures, due to the few percents of UV-A wavelength present in the solar spectrum, leading to a long distance photogenerated charge transfer, i.e. a charge transfer than can occur over a wide chain of particles. In the contrary, under visible light illumination, only rutile TiO_2 and WO_3 were activated due to a narrow band gap compared to anatase TiO_2, what led to a less extended charge transfer, mainly concerning photogenerated holes. This concept is interesting both for visible and solar-light activation (Fig. 7). Indeed, coupling different kinds of semi-conductors having adequate redox potentials for their valence and conduction bands, in terms of energy and respective level disposition leads to the formation of heterojunctions at the nano scale and consequently to photogenerated charge transfer, thus limiting the carrier recombination.

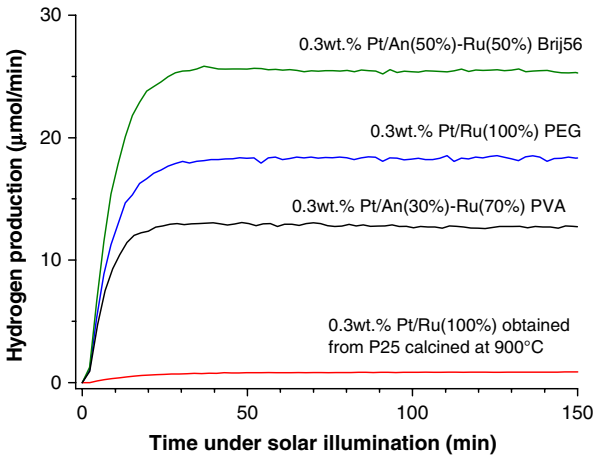

Fig. 6 150 W solar-light H_2 production from H_2O photocatalytic-dissociation over Pt(0.3 wt.%)/TiO_2. Reaction conditions: 2 g of photocatalyst dispersed in 750 mL of water. 110 mL/min of flowing N_2 stream. Methanol-to-water volume ratio of 1:15

This interparticle electron transfer (IPET) phenomena can subsequently increase the photooxidative or photoreductive efficency, as first reported by Serpone et al. and subsequently by many authors [25, 26]. Two kinds of coupling occur, (i) involving a one way vectorial electron transfer from a light activated semiconductor to a non-activated one, or (ii) leading to reciprocal electron and hole movements from simultaneously light activated semiconductors. This explains well the advantage of a binary or ternary coupling in the case of pure visible light and solar light activation (UVA + visible light). It must be pointed out that the presence of both anatase and rutile TiO_2 in suitable contents is positive for enhancing the photocatalytic activity for a visible- and solar-light use. There is no evidence that this anatase-rutile ratio should be the same whatever the application, and a parametric study should be required for optimizing the binary or ternary coupling.

4 Conclusion

This study shows a simple way of obtaining efficient visible and solar-light low temperature rutile-anatase photocatalysts for a wide spectra of liquid and gas phase applications. The use of organic template porogens allowed high surface area binary and ternary coupled anatase/rutile-based photocatalytic systems to be obtained, and CO

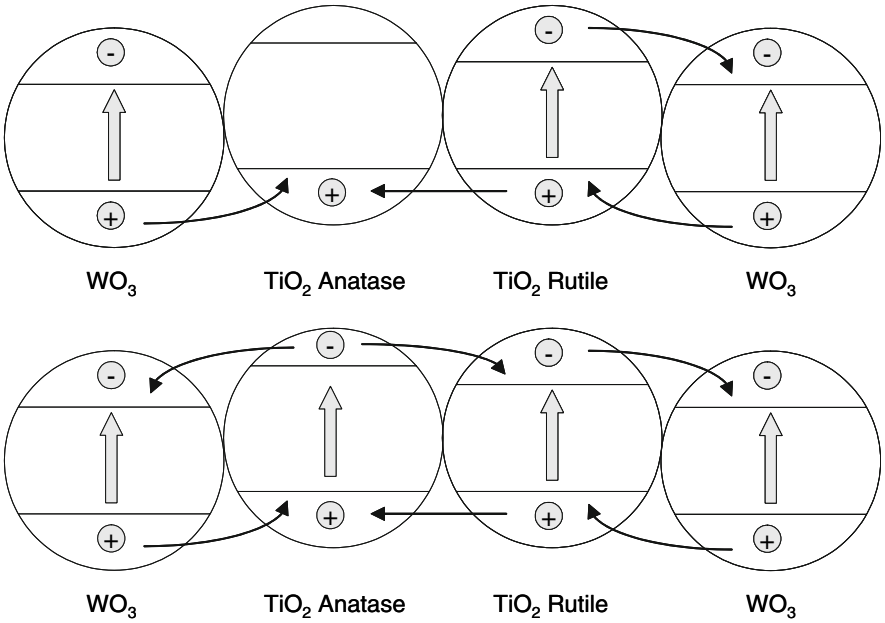

Fig. 7 Heterojunctions formation through semiconductor ternary coupling involving rutile, anatase and WO_3. One way and reciprocal charge transfer between activated and non-activated semiconductor oxides. *Top*: visible-light activation—*Bottom*: solar (UV-A + visible) light activation

oxidation, diethylsuflide degradation and hydrogen production were reported as examples. The photocatalytic performances, and especially those resulting from the beneficial binary and ternary semiconductor coupling, can be improved by simply tuning the anatase-rutile ratio, the porosity structuration and the specific surface area using different kinds of template porogens.

Acknowledgments The authors gratefully aknowledge the financial support of the Délégation Générale à l'Armement (DGA, Le Bouchet, France) and of the french Agence Nationale de la Recherche (ANR).

References

1. Anpo M (2000) Pure Appl Chem 388:431
2. Asahi R, Morikawa T, Ohwaki T, Oaki K, Taga Y (2001) Science 293:269
3. Limura S, Teduka H, Nakagawa A, Yoshihara S, Shirakashi T (2001) Electrochemistry 69(5):324
4. Fox MA, Dulay MT (1996) Chem Rev 93:341
5. Li Y, Lee N, Lee E, Song J, Kim S (2004) Chem Phys Lett 389:124
6. Anpo M, Shima T, Kodoma S, Kubokawa Y (1987) J Phys Chem 91:4305
7. Zhan H, Banfield JF (2000) J Phys Chem B 104:3481
8. Wu M, Lin G, Chen D, Wang G, He D, Feng S, Xu R (2002) Chem Mater 14:1974
9. Hu ZS, Dong JX, Chen GX (1999) Powder Technol 101:205
10. Bosc F, Ayral A, Keller N, Keller V (2007) Appl Catal B: Environ 69:133
11. Tang Z, Zhang J, Cheng Z, Zhang Z (2002) Mater Chem Phys 77:314
12. Yin S, Hasegawa H, Maeda D, Ishitsuba M, Sato T (2004) J Photochem Photobiol A: Chem 163:1
13. Bu SJ, Jin ZG, Liu XX, Yang LR, Cheng ZJ (2005) J Eur Ceram Soc 25:673
14. Soler-Illia GJdeAA, Louis A, Sanchez C (2002) Chem Mater 14:750
15. Yang P, Zhao D, Margolese DI, Chmelka BF, Stucky GD (1998) Nature 396:152
16. Zhen J, Pang JB, Qui KY, Wie Y (2001) J Mat Chem 11:3367
17. Robert D (2007) Catal Today 122(1–2):20
18. Gao B, Ma Y, Cao Y, Yang W, Yao J (2006) J Phys Chem B 110:14391
19. Keller V, Garin F (2003) Catal Commun 4:377
20. Abe R, Sayama K, Domen K, Arakawa H (2001) Chem Phys Lett 344:339
21. Wu C, Yue Y, Deng X, Hua W, Gao Z (2004) Catal Today 93–95:863
22. Di Paola A, Palmisano L, Augugliaro V (2000) Catal Today 58:141
23. Linsebigler AL, Lu G, Yates JT Jr (1995) Chem Rev 95:735
24. Zhang M, Jin Z, Zhang J, Zhang Z, Dang H (2005) J Mol Catal A: Chem 225:59
25. Serpone N, Maruthamuthu P, Pichat P, Pelizetti E, Hidaka H (1995) J Photochem Photobiol A: Chem 85:247
26. Bessoukhouad Y, Robert D, Weber J-V (2005) 101:315